



UNIVERSIDAD AUTÓNOMA DE SAN LUIS POTOSÍ

FACULTAD DE CIENCIAS QUÍMICAS

PROGRAMA DE POSGRADO EN BIOPROCESOS

**DIAGRAMAS DE FASE DE MEZCLAS DE
N-HENTRIACONTANO Y TRIACILGLICÉRIDOS
MONOÁCIDOS SATURADOS**

OPCIÓN DE TITULACIÓN:
ARTÍCULO DE INVESTIGACIÓN QUE PARA OBTENER EL GRADO DE
MAESTRO EN CIENCIAS EN BIOPROCESOS

PRESENTA:

I.A. CECILIA TAPIA LEDESMA

DIRECTOR DE TESIS:

DR. JAIME DAVID PÉREZ MARTÍNEZ

SAN LUIS POTOSÍ, S. L. P.

Agosto, 2019

El programa de Maestría en Ciencias en Bioprocesos de la
Universidad Autónoma de San Luis Potosí
Pertenece al Programa Nacional de Posgrados de Calidad (PNPC)
del CONACyT, registro 000588 en el Nivel Maestría (Consolidado).

Proyecto realizado en:

Laboratorio de Biopolímeros alimentarios de la Facultad de
Ciencias Químicas de la Universidad Autónoma de San Luis
Potosí.

Con financiamiento de:

El Consejo Nacional de Ciencia y Tecnología (CONACYT) mediante
la beca nacional para estudios de posgrado con número de registro
618723, otorgada a la I.A. Cecilia Tapia Ledesma.

El Consejo Nacional de Ciencia y Tecnología de México
(CONACYT) a través del Fondo Sectorial para la Educación
(Investigación Básica SEP-CONACYT, No: 256100).

Agradecimientos Académicos

A mi director de tesis, el Dr. Jaime David Pérez Martínez, por su apoyo, confianza, paciencia, consejos y motivación. Por todo su tiempo y dedicación en el desarrollo de este proyecto de investigación.

A la Dra. Elena Dibildox Alvarado, por su apoyo en el préstamo de los equipo de caracterización, por sus asesorías y por compartir siempre sus conocimientos.

A la Dra. Claudia Álvarez Salas, por siempre brindarme su confianza y apoyarme en todo momento.

A la Dra. Sandra Araujo Díaz, por apoyarme en la realización de experimentos, su apoyo en la revisión de la tesis y por brindarme siempre una mano amiga.

A mis sinodales, Dr. Miguel Ruiz Cabrera, Dr. Elena Dibildox Alvarado por sus valiosos comentarios y aportaciones al proyecto.

Al Dr. Alejandro Estrada Baltazar, por su colaboración, conocimientos, disposición y apoyo durante mi estancia nacional en el Tecnológico Nacional de Celaya.

A mis compañeros y amigos del laboratorio de biopolímeros alimentarios por su apoyo incondicional.

Al Consejo Nacional de Ciencia y Tecnología (CONACyT) por la beca otorgada para la realización de mis estudios de maestría.

Agradecimientos Personales

A Dios, por permitirme concluir una etapa más en mi vida.

A mis padres, mi principal motor en la vida. Sin ustedes esto no hubiera sido posible. Gracias por su apoyo incondicional, por heredarme valores, por ser mi ejemplo a seguir. Gracias por todo el amor que me brindan, eternamente les estaré agradecida. Las palabras no me bastarían para expresar el inmenso amor que tengo por ustedes.

A mis hermanas, Laura y Cris, gracias por acompañarme en cada proyecto y decisión, por sus consejos y motivación. Por ser mis compañeras de vida.

A mis amigos de la vida, Brisa, Chely, Gisie, Leo, Sandy, Jessy, Martita, Mechu, Kika, Saide, Sarai, Eder, Jeo, Rubén, es un honor contar con su amistad.

A las amistades que forme durante la maestría: Malu, Dánae, Ana, Allison, Angie, Lili, Suli, Hansel, Edgar, Pao, Lili. Gracias por sus palabras de aliento, motivación, gracias por todo lo compartido.

A todos mis amigos y compañeros de biopolímeros: Sandra, Viry, Diego, Gaby, Adri, Juliana, Nayeli, Saide, Marisol, Janin, Karen, Andrés, Edith, Hazel, Raquel, Estelita. Gracias por todo lo vivido, fue muy agradable trabajar con ustedes. Y por todo el apoyo que me brindaron.

A Fundación Juan Pablo, mis días se llenaron de luz y vida cuando llegue el Rincón de Juan Pablo. Gracias Marce, Marité, Rosy, Ceci, Maricruz, Mariana por tantas muestras de apoyo y cariño. A todos mis amigos voluntarios, gracias por escucharme y por tantos momentos compartidos: Javo, Sofí, Vane, Eli, Marifer, Camila, Susy, Osiel.

Gracias a todos los que formaron parte de este sueño.

Tabla de contenido

HIGHLIGHTS	1
RESUMEN	2
ABSTRACT	3
1. INTRODUCTION	6
2. MATERIALS AND METHODS	9
2.1. MATERIALS.....	9
2.2. METHODS.....	9
2.2.1. DIFFERENTIAL SCANNING CALORIMETRY.....	9
2.2.2. WIDE-ANGLE X-RAY DIFFRACTION.....	10
2.2.3. POLARIZED LIGHT MICROSCOPY.....	10
2.3. STATISTICAL ANALYSIS.....	11
3. RESULTS AND DISCUSSION	11
3.1 PURE COMPONENTS.....	11
3.2. <i>N</i> -HENTRIACONTANE/TAGS MIXTURES.....	12
3.2.1. DYNAMIC CRYSTALLIZATION.....	12
3.2.2. TAG MIXTURES ANNEALING.....	13
3.2.3. SOLID-LIQUID PHASE DIAGRAMS.....	14
3.2.3.1. <i>N</i> -HENTRIACONTANE – TRIMIRISTIN.....	14
3.2.3.2. <i>N</i> -HENTRIACONTANE - TRIPALMITIN.....	15
3.2.3.3. <i>N</i> -HENTRIACONTANE – TRISTEARIN.....	16
4. CONCLUSIONS	17
REFERENCES	21

HIGHLIGHTS

- *n*-hentriacontane (C31) and monoacid saturated TAGs had eutectic mixtures
- The eutectic composition changed as a function of the TAG melting temperature
- In mixtures, C31 had a major effect on TAG's crystals microstructure
- Microstructural changes for trimiristin were driven by heterogeneous nucleation
- Microstructural changes for tripalmitin were driven by crystal growth inhibition
- Microstructural changes for tristearin were driven by crystal growth inhibition

Resumen

La gelificación de aceite vegetal con cera de candelilla (CW) y triacilgliceroles saturados (TAGs) es una estrategia prometedora para el desarrollo de bases grasas, cosméticos y sistemas de liberación de medicamentos. El *n*-hentriacontano (C31) define, en gran medida, las propiedades térmicas de CW. Por lo tanto, estudiamos el comportamiento de fase y la microestructura de las mezclas binarias de C31 y trimiristina (MMM), tripalmitina (PPP) o triestearina (SSS), que proporcionarán la base para comprender las mezclas complejas que los contienen. Mediante calorimetría diferencial de barrido y difracción de rayos X se desarrollaron diagramas de fase para sistemas binarios C31-TAG. Estos diagramas de fase presentaron un comportamiento de fase eutéctica, en el que las mezclas de C31-TAG por debajo de la línea sólida son dispersiones sólidas de cristales ricos en C31 y cristales ricos en el correspondiente TAG. Dicha segregación en la fase sólida se atribuyó a la incompatibilidad del empaquetamiento de subcelda de los componentes puros en la forma polimórfica estable, la cual es ortorrómbica para C31, y monoclinica para TAG en la forma polimórfica β . El C31 en las mezclas tuvo un efecto importante en la microestructura de TAGs. Para la MMM, los cambios morfológicos a nivel microestructural fueron impulsados por su nucleación heterogénea en la superficie de los cristales de C31. En contraste, los cambios microestructurales para los cristales de los TAGs en las mezclas de C31-PPP y C31-SSS fueron inducidos por la inhibición del crecimiento del cristal por adsorción de moléculas de C31 en las superficies del cristal en crecimiento.

Palabras clave: Diagrama de fase, equilibrio sólido-líquido, *n*-hentriacontano, triestearina, tripalmitina, trimiristina, triacilgliceroles saturados, cera de candelilla, oleogeles.

Abstract

Gelation of vegetable oil with candelilla wax (CW) and saturated triacylglycerols (TAGs) is a promising strategy for engineering solid-like fat-based foods, cosmetics, and drug delivery systems *n*-hentriacontane (C31) defines, to a large extent, the thermal properties of CW. Therefore, we studied the phase behavior and microstructure of binary mixtures of C31 and trimyristin (MMM), tripalmitin (PPP) or tristearin (SSS), which will provide the basis to understand complex mixtures. Through differential scanning calorimetry and X-ray diffraction the phase diagrams for C31-TAG binary systems were developed. These phase diagrams had a eutectic phase behavior, in which C31-TAG mixtures below the solidus line are solid dispersions of crystals rich in C31, and crystals rich in the corresponding TAG. Such segregation in the solid phase was attributed to the incompatible subcell-packing of the pure components in the stable polymorphic form, which is orthorhombic for C31, and monoclinic for TAGs in the β -polymorphic form. C31 in mixtures had a major effect on the TAGs microstructure. For MMM, morphological changes at the microstructural level were driven by its heterogeneous nucleation on C31 crystals. Conversely, microstructural changes for TAGs crystals in C31-PPP and C31-SSS mixtures were induced by the crystal growth inhibition by adsorption of C31 molecules at the growing crystal surfaces.

Keywords: Phase diagram, solid-liquid equilibrium, *n*-hentriacontane, tristearin, tripalmitin, trimyristin, saturated triacylglycerols, candelilla wax, oleogels.

Submission Confirmation

Ref: TCA_2019_593

Title: Phase diagrams of mixtures of n-hentriacontane and saturated monoacid triacylglycerols

Journal: Thermochemica Acta

Dear Dr. Pérez-Martínez,

Thank you for submitting your manuscript for consideration for publication in Thermochemica Acta. Your submission was received in good order.

To track the status of your manuscript, please log into EVISE® at: http://www.evise.com/evise/faces/pages/navigation/NavController.jspx?JRNL_ACR=TCA and locate your submission under the header 'My Submissions with Journal' on your 'My Author Tasks' view.

Thank you for submitting your work to this journal.

Kind regards,

Thermochemica Acta

Phase diagrams of mixtures of *n*-hentriacontane and saturated monoacid triacylglycerols

Tapia-Ledesma C.^a, Araujo-Díaz S. B.^a, Dibildox-Alvarado E.^a, Ornelas-Paz J. de J.^b, Pérez-Martínez J. D.^{a*}

^a Facultad de Ciencias Químicas, Centro de Investigación y Estudios de Posgrado, Universidad Autónoma de San Luis Potosí, San Luis Potosí, 78210, Mexico

^b Centro de Investigación en Alimentación y Desarrollo, A.C. Unidad Cuauhtémoc, Av. Río Conchos S/N, Parque Industrial, 31570, Mexico

† Electronic supplemental file

* Corresponding author.

Tel: + 52 444 8262440 ext. 6432

E-mail: j davidperez@uaslp.mx (Jaime David Pérez-Martínez)

Mailing address:

Facultad de Ciencias Químicas-CIEP

Zona Universitaria

Av. Dr. Manuel Nava 6, Zona Universitaria

San Luis Potosí, SLP 78210, México.

1. INTRODUCTION

The relationship between different scales of structure, physical properties, and stability, is of paramount relevance to develop new matrices for foods, pharmaceutical vehicles, or cosmetic products (Marangoni et al., 2012). The micro and mesostructural features of systems structured by a crystal network, as plastic fats and oleogels, define several macroscopic properties like the system elasticity, yield stress, optical transparency, liquid binding capacity, and diffusivity (Sánchez-Becerril et al., 2018; Blake, Co, & Marangoni, 2014). On the other hand, the molecular structure and thermodynamic properties of the solid phase are determinant to predict the gel stability, the gelator solubility, and the processing conditions in general (Toro Vazquez & Pérez Martínez, 2018). Thus, the design of stable oleogels and plastic fats requires a full understanding of the interactions among different species at the molecular packing level. Such interactions can be understood from the phase behavior and crystal ripening process of pure neat gelators and their mixtures (Abdallah & Weiss, 2000; Ostuni, Kamaras, & Weiss, 1996; Serrato-Palacios et al., 2015; Toro-Vazquez et al., 2007).

Edible oleogels are typically structured with low molecular weight gelators including steroids, plant sterols, tri-, di-, and monoglycerides, and natural waxes (Yang et al., 2017). Among this gelators, waxes stand out, as these can produce thermoreversible oleogels at very low concentrations (as low as 0.5 wt.%) (Patel, 2015; Blake et al., 2014). Natural waxes are complex mixtures of wax esters, hydrocarbons, fatty acids, fatty alcohols, phenolic esters, among others. Most studied waxes include rice bran wax, sunflower wax, sugarcane wax, beeswax and candelilla wax (CW) (Blake et al., 2014). Thermodynamically stable oleogels with excellent oil binding capacity can be produced using $\geq 1\%$ CW, nevertheless, the rheological properties of these gels do not match the requirements for several edible applications. Typically, these oleogels are too soft to produce stick margarines, spreads, and confectionery coatings (Blake et al., 2014; Dassanayake, Kodali, Ueno, & Sato, 2009; Hwang et al., 2013; Toro Vazquez et al., 2007). In this regard, wax content can be increased to harden the oleogels but, this will also increase the gel's melting temperature, causing a pasty mouthfeel which negatively affects the

sensorial properties (Hwang et al., 2013; Zetl & Marangoni, 2014). To overcome these limitations, Chopin-Doroteo et al., (2011) added 1% tripalmitin (PPP) to 3% CW vegetable oil solutions, producing composite oleogels with higher elasticity and yield stress than 3% CW gels produced without PPP while the melting temperature was maintained between 36 to 38 °C. The elasticity increment was associated with the CW and PPP co-crystallization, as the distinctive PPP spherulites were not spotted by polarized microscopy, neither detected by X-ray diffraction. More recently, Ramírez-Gómez et al. (2016), produced composite oleogels with CW and saturated triacylglycerols (TAGs) from fully hydrogenated soybean oil (FH). They observed a synergistic effect of FH and CW on the systems' elasticity (i.e., G'), and a positive effect of FH on the mechanical reversibility of CW gels. Nonetheless, the underlying mechanisms for the positive interaction between CW and saturated TAGs are not fully elucidated.

TAGs have a monotropic polymorphism, where all but one polymorph are unstable. For these compounds, crystallization kinetics leads to the formation of unstable or metastable polymorphs (i.e., α or β') that spontaneously will transform to the stable polymorph β (Small, 1986; Walstra, 2003). The unstable α polymorph has a hexagonal subcell packing where the hydrocarbon chains molecules are perpendicular to the lamellar plane, while the metastable β' polymorph has an orthorhombic subcell packing where the hydrocarbon chains are inclined 108° with respect to the plane. On the other hand, the stable β polymorph has a triclinic subcell packing with a hydrocarbon chain inclined 128°. In this research we analyze mixtures of *n*-hentriacontane with trimyristin (MMM), tripalmitin and tristearin (SSS); a series of trisaturated TAGs found in high melting natural fats (i.e., nutmeg, palm oil) and/or fully hydrogenated vegetable oils (Da Silva et al., 2016; Frank, Roberts, Snell, Yates, & Collins, 1971; Son et al., 2010). The phase behavior of these components is found elsewhere (Da Silva et al., 2016; Haghshenas, Smith, & Bergenståhl, 2001; Hong et al., 2012; Kellens, Meeussen, & Reynaers, 1992; Sato, 2001; Timms, 1984).

Main CW components are *n*-alkanes with odd number of carbons from C₂₉ to C₃₃ (47.3%) and *n*-hentriacontane (C₃₁H₆₄, 35.5%) as the major constituent. Other components include triterpenic alcohols (24.8%), fatty acids with even number of carbons from C₂₆ to C₃₄ (16.6%), fatty alcohols with even number of carbons from C₂₈ to C₃₄ (3.61%), and esters from C₃₉ to C₆₄ (5.83%) (Toro-Vazquez et al., 2013). Despite the large number of components, the crystallization, gelation, and physical properties exhibited by CW in vegetable oil are determined to a great extent by its major constituent, *n*-hentriacontane (C₃₁) (Serrato-Palacios et al., 2015; Toro-Vazquez et al., 2013). Pure *n*-alkanes phase behavior is determined by three parameters: temperature, carbon atom number, and parity of the hydrocarbon chain. The crystal packing of solid phases of *n*-alkanes can be grouped in ordered and disordered polymorphs. The subcell structure of ordered polymorphs includes triclinic, monoclinic, orthorhombic, while disordered polymorphs are triclinic disorder phase, monoclinic disorder phase, orthorhombic rotator phase and the rhombohedral rotator phase (Briard, Bouroukba, Petitjean, Hubert & Dirand, 2003). Odd numbered *n*-alkanes with 9-69 carbons has an orthorhombic crystal structure at low temperature, while even numbered has a triclinic for 6-26 carbons, monoclinic for 28-36 carbons and orthorhombic for 38-44 carbons. In every case, the increase in temperature below the melting point originates solid-solid polymorphic transitions of the type order-order and order-disorder transitions (Dirand et al., 2002). Besides, the polymorphism of *n*-alkanes can be modified when small amounts (< 2%) of impurities are introduced in their crystal lattice, or when is crystallized from solutions (Abdallah & Weiss, 2000; Serrato-Palacios et al., 2015; Shearer & Vand, 1956).

Despite the molecular self-assembly of neat gelators might differ from that in the three-dimensional crystal network of oleogels, the phase behavior of binary mixtures of long-chain *n*-alkanes and TAGs can provide valuable information to engineer composite oleogels with mixtures of CW and TAGs with specific melting properties and improved rheology. To the best of our knowledge, there is no information regarding the phase behavior and microstructural characterization for these mixtures. Within this context, the objective of this work was to develop the phase diagrams of neat binary mixtures of *n*-hentriacontane and MMM, PPP or SSS

using differential scanning calorimetry and X-ray diffraction, and complement the diagrams with microstructural features.

2. MATERIALS AND METHODS

2.1. MATERIALS

n-hentriacontane (C31) was obtained from Santa Cruz Biotechnology ($\geq 95\%$ purity), and the saturated monoacid TAGs (MMM, PPP, and SSS) were from Sigma-Aldrich (purity $\geq 99\%$). Mixtures (C31-TAG) were prepared weighing the corresponding amount of each compound in a sample container, heating at 20 °C above the highest melting compound for 10 min, stirring with a micro spatula to produce a homogeneous melt, cooling at room temperature, and processing according to the methods described in Sections 2.2.1, 2.2.2, and 2.2.3. Mixtures were prepared in molar fraction ratio.

2.2. METHODS

2.2.1. DIFFERENTIAL SCANNING CALORIMETRY

Crystallization and melting profiles of pure components and mixtures were determined using a differential scanning calorimeter (model 2920; TA Instruments New Castle, DE, USA) equipped with a refrigerated cooling unit. The DSC was calibrated with indium (melting temperature of 156.6 °C, melting enthalpy of 28.45 J/g), and an empty aluminum pan was used as a reference. The DSC cell was purged with chromatographic grade nitrogen ($\geq 99.99\%$ purity; 15 mL/min). Samples weighed in aluminum pans were processed as described in Section 2.1, hermetically sealed, and placed in the measuring cell. Pure compound and their mixtures were heated to 95 °C for 20 min, cooled (5 °C/min) to 0 °C and maintained isothermally for 2 min. After that, the system was heated (5 °C/min) to 20 °C above the system melting temperature. Samples showing recrystallization during this heating step were annealed to eliminate unstable polymorphs. The annealing process consisted of heating to 95 °C for 20 min, cooling (5 °C/min) to 0 °C, kept isothermal for 2 min, heating (5 °C/min) to the recrystallization temperature for 5 min, and cooling (5 °C/min) to 0 °C for 2 min. After that, the annealed sample was heated (5 °C/min) to 95

°C to obtain the melting thermogram. To improve the peaks resolution, the final heating of annealed samples was also performed a 1°C/min for pure compounds and mixtures showing a single melting peak. The thermal parameters measured were temperatures of onset (T_{oi}) and peak (T_{ci}) of each compound detected in the first cooling thermogram, as well as the enthalpy (ΔH_{mi}), peak (T_{mi}) and end point (T_{ei}) of each melting compound, and the temperature peak of the order-disorder transition of C31 (T_{od}) obtained from the heating thermogram of annealed samples. These parameters were assessed using the first derivate of heat flow with software equipment (Universal Analysis 2000 Ver. 4.2E; TA Instruments-Waters LLC).

2.2.2. WIDE-ANGLE X-RAY DIFFRACTION

Wide-angle X-ray diffraction patterns (WAX) of pure components and their mixtures were analyzed using an X-ray diffractometer (Panalytical, X'Pert Pro, Almelo, The Netherlands) equipped with a CuKaR source ($\lambda = 1.54 \text{ \AA}$) excited at 35 kV and 30 mA, 0.5° divergence slit, 1° scatter slit, and 5.5 mm receiving slit. Samples were placed in an aluminum sample holder ($\approx 500 \text{ mg}$), molten and annealed according to Section 2.2.1. After that, the annealed sample was stored at 25 °C for 24 h. The temperature program was controlled with the software Rheoplus/32 V3.61 (Anton-Paar, Germany), and applied with a Peltier plate (P-PTD200/62/TG, Anton-Paar, Germany) on the bottom of the sample holder and a Peltier hood (H-PTD-200, Anton-Paar, Germany) on the top. To avoid the crystallites preferential orientation, samples were finely grated at room temperature before analysis. The diffraction patterns were obtained by scanning the samples from 3° to 35° using a step of 0.02° and a scanning speed of 0.04 °/min. Diffraction patterns were collected by the X'Pert Data Collector software version 2.0. The X-ray diffraction analysis was carried out for pure compounds and three mixtures of each binary system.

2.2.3. POLARIZED LIGHT MICROSCOPY

Microphotographs of pure compounds and binary mixtures were obtained with a polarized light microscope ECLIPSE LV100N POL (Nikon, Japan), equipped with a digital color video camera Micropublisher 3.3 RTV Q (QImaging, Canada) and a

temperature-controlled stage (Lynkam Scientific Instruments LTS420, UK) connected to a liquid nitrogen pumping system (Lynkam Scientific Instruments LNP95, UK). The temperature program was controlled with the software Linksys 32 ver. 2.3.0 (Lynkam Scientific Instruments LTD, UK). Samples (≈ 10 mg) were placed on a glass slide and heated to 95 °C and stirred with a micro-spatula, after that a coverslip was placed on the molten sample. Samples were processed according to the annealing program described in Section 2.2.1. Microphotographs of samples at 25 °C were collected with the software NIS-Elements AR 4.51 (Nikon, Japan).

2.3. STATISTICAL ANALYSIS

Plots were done with Prism 5.0 software (GraphPad Software Inc. San Diego, CA, USA). Statistical analysis for the effect of C31 molar fraction was performed by one-way ANOVA ($P < 0.05$) for each mixture using STATISTICA V 7.1 (StatSoft, Inc. Tulsa, OK).

3. RESULTS AND DISCUSSION

3.1 PURE COMPONENTS

The cooling/heating thermograms for the pure TAGs (*i.e.*, MMM, PPP and SSS) and C31 are shown in Fig.1. During cooling of the molten, TAGs presented just one crystallization exotherm (Fig. 1A), while the corresponding heating thermograms (Fig. 1B) showed one recrystallization exotherm and two endotherms for each TAG. Based on previous reports, the lower endothermic peak was associated with the melting of the α -form crystals, and the other to those in β -form (Hartel, von Elbe, & Hofberger, 2018). The recrystallization corresponded to the $\alpha \rightarrow \beta$ polymorphic transformation. To develop the phase diagrams, all compounds must be at equilibrium (*i.e.*, β -form for TAGs). After the annealing process, the heating thermograms of TAGs showed a single melting endotherm (Fig. 2A). The melting temperature and melting enthalpy agreed with those for the β -form reported elsewhere for these TAGs (Table 1; Hartel, von Elbe, & Hofberger, 2018; Da Silva et al., 2009; Matovic., 2005; Kolbe et al., 1999; Kellens & Reynaers., 20009). The β form in the annealed TAGs was corroborated with the X-ray diffractograms obtained at 25 °C, where the diffraction pattern showed three peaks in the wide angle region

($2\theta > 19^\circ$) at d values of 4.6 Å, 3.7 Å and 3.9 Å (Fig. 2B), which are distinctive of a triclinic subcell (Silva et al., 2014).

Given the enantiotropic polymorphism of C31, the heating thermogram of this compound showed the same endothermic transitions after crystallization of the molten, and after applying the annealing treatment used for SSS (Fig. 1B & Fig. 2A). The lower temperature endothermic peak was associated with the orthorhombic \rightarrow rotor phase transition ($T_{od,C31} = 61.55 \pm 0.35$ °C) and the higher temperature endotherm to the rotor phase \rightarrow liquid transition ($T_{m,C31} = 67.82 \pm 0.56$ °C). The enthalpy associated with the $o-d$ transition and the melting (222.70 ± 4.53 °C), and both temperature transitions were consistent with the reported data (Briard et al., 2003; Serrato-Palacios et al., 2018). The X-ray diffractogram of C31 showed two peaks of high intensity at d values of 4.2 and 3.8 Å (Fig 2B), characteristic the orthorhombic packing subcell, which is the stable form at 25 °C.

The crystal microstructure of the annealed compounds obtained by PLM is shown in Fig. 3. C31 is shown as large birefringent fibers much larger than those reported by Serrato-Palacios et al. (2015), which was attributed to the recrystallization process occurred during the annealing (Fig. 3A). On the other hand, the three TAGs observed spherulites with the typical Maltese cross shape in different sizes. PPP produced the larger crystals of this type, SSS had the smaller ones, while MMM had an intermediate size. In between of some Maltese cross-shaped crystals of MMM was a circle of granular microcrystals of very small size (Fig. 3B). This type of structures could be associated with the recrystallization occurring during de annealing process (Magill, 2001).

3.2. N-HENTRIACONTANE/TAGS MIXTURES

3.2.1 DYNAMIC CRYSTALLIZATION

The cooling thermograms of molten C31-TAG mixtures are shown in Fig. 4. Independently of the mixture composition, C31 crystallized to the highest temperature, showing a decline in the crystallization onset ($T_{o,C31}$) proportional to X_{C31} (Fig. S2). Thus, independently of the chain length, there was an evident dilution effect of these TAGs on C31. For the C31-MMM mixtures, the C31 crystallization

was detected all along of the concentration range. The C31 exotherm of systems with $X_{C31} = 1.0-0.60$ had two overlapping peaks associated with crystallization from the isotropic liquid \rightarrow rotor phase, and the rotor phase \rightarrow orthorhombic transition. On the other hand, C31 exotherms for systems with $X_{C31} = 0.5-0.05$ only evidenced the peak corresponding to the transition from the liquid \rightarrow orthorhombic phase (Serrato-Palacios *et al.* 2015). The same trend was observed in mixtures with the higher melting TAGs, but the C31 exotherms were detected only in systems with an $X_{C31} = 1.0-0.30$ or $X_{C31} = 1.0-0.20$ for mixtures with PPP or SSS, respectively. TAGs crystallization in mixtures were different for each mixture. In mixtures with MMM, the C31 increased the $T_{o,MMM}$ ($P < 0.05$) approximately 6 °C with respect to that of pure MMM (Fig. 4A). These results agreed with the seeding effect of sunflower wax on anhydrous milk fat (AMF), which reduced the induction time to nucleation, and increased the number of AMF crystals (Kerr, Tombokan, Ghosh & Martini, 2011; Martini, Carelli, & Lee, 2008). Thus, we concluded that C31 crystals acted as hetero-nuclei for MMM. In contrast to the C31-MMM mixture, the C31 crystals did not change ($P < 0.005$) the $T_{o,PPP}$, and had a slightly negative effect ($P < 0.05$) on the $T_{o,SSS}$ when compared with the corresponding pure component (Fig. 4B & 4C). This behavior is consistent with Ramírez-Gómez *et al.* (2016), where mixtures with different ratios of candelilla wax and fully hydrogenated soybean oil (FH) shown neither significant changes nor a slight depression in the crystallization onset of FH as the CW in the system increased. Considering the FH is mainly constituted SSS and other medium chain trisaturated TAGS, we concluded that the C31 crystals do not act as hetero-nuclei under dynamic crystallization conditions for PPP and SSS.

3.2.2 TAG MIXTURES ANNEALING

The heating thermograms from C31-TAG mixtures crystallized under dynamic cooling conditions showed recrystallization events associated with polymorphic transformations of unstable forms of TAGs (Fig. S3). As materials must be in equilibrium to construct phase diagrams, all mixtures were annealed to produce systems with TAGs crystals in the stable β -form, and C31 in the orthorhombic subcell packing. Regardless of the mixture composition, the XRD diffraction patterns from annealed C31-TAG mixtures showed the three distinctive peaks of the triclinic

subcell of TAGs in the β -form (Fig. 5) and the most intense peak of C31. The peak of C31 diffracting at 3.8 Å could not be detected as it is relatively less intense than the peaks at 3.7 and 3.9 Å produced from TAGs crystals in the β -form. Thus, we confirmed the annealed mixtures were thermodynamically stable, and that in all cases they were constituted by a mixture of TAG and C31 crystals.

3.2.3 SOLID-LIQUID PHASE DIAGRAMS

Melting endotherms of annealed mixtures of C31-TAG (Fig. 6) were used to construct solid-liquid equilibrium diagrams as a function of temperature and composition. These diagrams have liquid (L), solid-liquid equilibrium (SLE), and solid (S) regions. The *liquidus* line, separating the L region from the SLE region, were constructed with the melting peak $T_{m,i}$ of the highest melting compound in the mixture; while the *solidus* line corresponded to the $T_{m,i}$ of the lowest melting compound in the mixture. The *o-d* solid transition line of C31 was traced with the corresponding endotherm peak ($T_{od,C31}$).

3.2.3.1 N-HENTRIACONTANE – TRIMIRISTIN

The heating thermograms of annealed mixtures (Fig. 6) showed up to three endothermic peaks associated with the TAG melting, the o-d transition and melting of C31. For C31-MMM system, the highest temperature endotherm, corresponding to the melting of C31, were detected for systems with $X_{C31} = 1-0.3$ (Fig. 6A). Within this composition range, $T_{m,C31}$ decreased with the amount of C31 in the mixture. On the other hand, the endotherm of C31 o-d transition was identified systems with $X_{C31} = 1-0.5$ at 61.5 °C independently of the mixture composition. The lower melting endotherm, corresponding to MMM crystals, were detected in all mixtures. In contrast with $T_{m,C31}$, $T_{m,MMM}$ had only slight changes with the system composition. It is worth to note that, the single endotherm detected for C31-MMM mixtures with $X_{C31} \leq 0.3$ (Fig. 6A, Fig. S4A) was attributed to the concomitant melting of β -MMM and C31 crystals, as both crystals species were detected in the X-ray diffractograms (Fig. 5A). Phase change temperatures (*i.e.*, $T_{m,i}$, $T_{od,i}$) used to draw the delimiting lines in the C31-MMM phase diagram are in Table 2. From these data, the *liquidus* line (solid line in Fig. 7), corresponding to $T_{m,i}$ of the highest melting compound in

the mixture ($T_{m,C31}$ or $T_{m,MMM}$), exhibited an eutetic at $X_{C31} = 0.2$ with $T_m = 56.30$ °C. Below the *solidus* line, corresponding to the temperature of the melting peak of MMM ($T_{m,MMM}$), the systems were a micro-heterogeneous dispersion of β -MMM and C31 crystals (Fig. 7). Two SLE regions were found in mixtures with $X_{C31} > 0.20$ above the *solidus* line and below the *o-d* transition temperature. In these regions, the liquid phase was a mixture of MMM and C31 crystals. C31 was in the orthorhombic polymorphic form (C31_{ss}-O) or in the rotor phase (C31_{ss}-R) if they were below or above the *o-d* transition temperature, respectively.

Crystal habit of the studied TAGs were greatly modified in the mixtures, while C31 crystals maintained its characteristic fiber shape (Figs. 3, 7-9). C31 modified the shape of MMM crystals, changing from the spherulitic to a grainy habit. Also exhibited a crystal size reduction with the increment of C31 in the mixture (Fig. 7). These phenomena were attributed to the secondary nucleation of MMM on the C31 crystals surface as detected from the cooling thermograms (Secc. 3.2.1).

3.2.3.2 N-HENTRIACONTANE – TRIPALMITIN

In the heating thermograms of C31-PPP with $X_{C31} > 0.50$, the highest melting component was C31 (Fig. 6B). In this system, the melting temperature of C31 decrease with the amount of C31 while the *o-d* transition appeared around 61.5 °C, and the melting peak of PPP was detected at ~60 °C. Mixtures with $0.3 \leq X_{C31} \leq 0.5$ presented only one endotherm with a single peak (Fig. 6B), which was attributed to the simultaneous melting of the two crystal species detected by XRD (C31 and β -PPP) (Fig. 5B). On the contrary, mixtures with $X_{C31} = 0.1-0.2$ showed one melting endotherm with two overlapping peaks, the highest peak in these mixtures corresponded to PPP. The phase change temperatures used to draw the delimiting lines in the C31-PPP phase diagram are in Table 3. From these data, the *liquidus* line (solid line in Fig. 8) revealed a eutectic at $X_{C31} = 0.4$ with $T_m = 60.32$ °C. The X-ray diffraction analysis confirmed that below the *solidus* line, these components were structured as a micro-heterogeneous dispersion of β -PPP and C31 crystals (Fig. 8). This mixture had three SLE regions, one in mixtures with $0.2 \leq X_{C31} \leq 0.3$, and two for those with $0.3 < X_{C31} < 0.95$. In the former case crystals of β -PPP and a

liquid phase were in equilibrium, while the later a liquid phase and C31_{ss}-O were found above the solidus line and below the $T_{od,C31}$, and a liquid phase and C31_{ss}-R above the $T_{od,C31}$ and below the *liquidus* line. The microstructure of PPP crystals in mixture with C31 showed the most significant changes with respect to the pure PPP.

The grainy crystals in C31-PPP mixtures were much smaller than those of pure PPP, C31-MMM and C31-SSS mixtures (Figs. 3, 8). Nonetheless, thermograms of C31-PPP mixtures did not show evidence of a secondary nucleation process (Secc. 3.2.1). Therefore, the huge crystal size reduction of PPP crystals could result from the inhibition of the crystal growth by adsorption of C31 at the surface of the growing crystals. This effect is produced when impurities (i.e., C31 molecules) in the crystallizing media are adsorbed at the crystal surface, hindering the incorporation of the crystallizing species (i.e., PPP), as this has to be displaced before the incorporation of PPP to the crystal lattice can occur (Hartel, 2001).

3.2.3.3 N-HENTRIACONTANE – TRISTEARIN

For C31-SSS system, the highest melting endotherm corresponded to SSS in those with $X_{C31} < 0.6$, and to C31 in mixtures with $X_{C31} > 0.8$ (Fig. 6C). On the other hand, mixtures with $0.6 \leq X_{C31} \leq 0.8$ showed only one endothermic peak, which was attributed to the concomitant melting of the C31 and β -SSS crystals as detected by XRD (Fig. 5C). From these data (Table 4), the *liquidus* line revealed a eutectic region at $0.6 \leq X_{C31} \leq 0.8$ with $T_m = 64$ °C (solid line in Fig. 9). As in the other systems, the melting temperature of C31 decrease with the amount of C31 while the *o-d* transition appeared around 61.5 °C, and the melting peak from SSS decrease to a minimum 63.87 °C. The solidus line corresponding to the melting of either C31 or β -SSS was practically an exothermic line at ~64 °C. Below this line and above $T_{od,C31}$, mixtures with $X_{C31} \geq 0.4$ coexist as a mixture of β -SSS and C31-R, but below $T_{od,C31}$ these systems consisted of a physical mixture of β -SSS and C31-O crystals (Fig. 9). Two SLE regions were identified for this system, one for mixtures with $X_{C31} < 0.6$ where β -SSS and a liquid phase coexist, and other for mixtures with $X_{C31} > 0.8$ where the C31-R was in equilibrium with the liquid phase.

The SSS crystal microstructure changed as a function of the C31 content in the mixture. At $X_{C31} = 0.1$, the spherulitic shape and crystal size were quite like that of pure SSS (Figs. 3, 9). On the other hand, mixtures with $X_{C31} \geq 0.4$ had grainy crystals, with slight changes in crystal size. As in C31-PPP mixtures, such morphological changes could not be associated with a secondary nucleation process (Secc. 3.2.1), but to the crystal growth inhibition by adsorption of C31 at the surface of the growing crystals. It is worth to mention that the size reduction of TAGs crystals induced by C31 is desirable for a number of lipid-based matrices for food, cosmetic and drug delivery products, as a smaller crystal size produces a smoother texture, and increases the product elasticity (Keer et al., 2011).

4. CONCLUSIONS

Mixtures of C31 and the TAGS here studied had a eutectic phase behavior. The eutectic composition was richer in the TAG as the melting temperature of the TAG increased; that is $X_{C31} = 0.2$, $X_{C31} = 0.4$, and $X_{C31} = 0.7-0.8$ for MMM, PPP, and SSS, respectively. Thus, below the solidus line these systems were a solid dispersion of crystals rich in C31 and crystals rich in the corresponding TAG. Such segregation in the solid phase was attributed to the difference in subcell-packing of the pure components stable polymorphic form, orthorhombic for C31, and monoclinic for TAGs in the β -polymorphic form. The microstructure of TAGs crystals was largely modified in mixtures with C31. Morphological changes in MMM crystals were driven by its heterogeneous nucleation on C31 crystals developed while mixtures were cooled from the molten. On the other hand, microstructural changes for TAGs crystals in mixtures with PPP and SSS in mixtures were driven by the crystal growth inhibition by adsorption of C31 molecules at the growing crystal surfaces.

ACKNOWLEDGMENTS

This research was funded by the National Council for Science and Technology of Mexico (CONACYT) through the Fondo Sectorial de Investigación para la Educación (Investigación Básica SEP-CONACYT; grant number: 256100).

CAPTIONS

Figure 1. Cooling (A) and heating (B) thermograms obtained at 5 °C/min for neat *n*-hentriacontane (C31), trimyristin (MMM), tripalmitin (PPP), and tristearin (SSS).

Figure 2 Heating thermograms obtained at 5 °C/min (A) and X-ray diffractograms (B) for annealed *n*-hentriacontane (C31), trimyristin (MMM), tripalmitin (PPP), and tristearin (SSS).

Figure 3 Polarized light microscopy images for annealed *n*-hentriacontane (A), trimyristin (B), tripalmitin (C), and tristearin (D).

Figure 4 Cooling thermograms obtained at 5 °C/min for mixtures of *n*-hentriacontane (C31) and trimyristin (A), tripalmitin (B), or tristearin (C). Mixtures composition are identified by the *n*-hentriacontane mole fraction (X_{C31}).

Figure 5 X-ray diffractograms for annealed for mixtures of *n*-hentriacontane (C31) and trimyristin (A), tripalmitin (B), or tristearin (C). Mixtures composition are identified by the *n*-hentriacontane mole fraction (X_{C31}).

Figure 6 Heating thermograms obtained at 5 °C/min for annealed mixtures of *n*-hentriacontane (C31) and trimyristin (A), tripalmitin (B), or tristearin (C). Mixtures composition are identified by the *n*-hentriacontane mole fraction (X_{C31}).

Figure 7 Phase diagram for *n*-hentriacontane (C31) and trimyristin (MMM) binary system and polarized light microphotographs of selected mixtures. Mixtures' composition is identified by the C31 mole fraction (X_{C31}). Melting peak temperatures for C31 and β -MMM, and the order-disorder transition for C31 are indicated in the graph. Liquid (L), crystal rich in trimyristin (β -

MMM), crystal rich in C31 in rotator phase (C31-R), crystal rich in C31 in orthorhombic phase (C31-O).

Figure 8 Phase diagram for *n*-hentriacontane (C31) and tripalmitin (PPP) binary system and polarized light microphotographs of selected mixtures. Mixtures' composition is identified by the C31 mole fraction (X_{C31}). Melting peak temperatures for C31 and β -PPP, and the order-disorder transition for C31 are indicated in the graph. Liquid (L), crystal rich in trimyristin (β -MMM), crystal rich in C31 in rotator phase (C31-R), crystal rich in C31 in orthorhombic phase (C31-O).

Figure 9 Phase diagram for *n*-hentriacontane (C31) and tristearin (SSS) binary system and polarized light microphotographs of selected mixtures. Mixtures' composition is identified by the C31 mole fraction (X_{C31}). Melting peak temperatures for C31 and β -SSS, and the order-disorder transition for C31 are indicated in the graph. Liquid (L), crystal rich in trimyristin (β -MMM), crystal rich in C31 in rotator phase (C31-R), crystal rich in C31 in orthorhombic phase (C31-O).

Figure S1. Heating thermograms obtained at 1 °C/min for annealed *n*-hentriacontane (C31), trimyristin (MMM), tripalmitin (PPP), and tristearin (SSS).

Figure S2. The crystallization onset of *n*-hentriacontane ($T_{o,C31}$) versus X_{C31} for mixtures of *n*-hentriacontane (C31) and trimyristin (MMM), tripalmitin (PPP), or tristearin (SSS).

Figure S3. Heating thermograms obtained at 5 °C/min for mixtures of *n*-hentriacontane (C31) and trimyristin (A), tripalmitin (B), or tristearin (C). Mixtures composition are identified by the *n*-hentriacontane mole fraction (X_{C31}).

Figure S4 Heating thermograms obtained at 1 °C/min for pure components and a selected number of annealed mixtures of *n*-hentriacontane (C31) and trimyristin (A), tripalmitin (B), or tristearin (C). Mixtures composition are identified by the *n*-hentriacontane mole fraction (X_{C31}).

REFERENCES

1. Abdallah, D. J., & Weiss, R. G. (2000). Organogels and low molecular mass organic gelators. *Advanced Materials*, 12(17), 1237–1247. [https://doi.org/10.1002/1521-4095\(200009\)12:17<1237::AID-ADMA1237>3.0.CO;2-B](https://doi.org/10.1002/1521-4095(200009)12:17<1237::AID-ADMA1237>3.0.CO;2-B)
2. Blake, A. I., Co, E. D., & Marangoni, A. G. (2014). Structure and physical properties of plant wax crystal networks and their relationship to oil binding capacity. *JAOCS, Journal of the American Oil Chemists' Society*, 91(6), 885–903. <https://doi.org/10.1007/s11746-014-2435-0>
3. Briard, A. J., Bouroukba, M., Petitjean, D., Hubert, N., & Dirand, M. (2003). Experimental enthalpy increments from the solid phases to the liquid phase of homologous n-alkane series (C18 to C38 and C41, C44, C46, C50, C54, and C60). *Journal of Chemical and Engineering Data*, 48(3), 497–513. <https://doi.org/10.1021/je0201368>
4. Chopin-Doroteo, M., Morales-Rueda, J. A., Dibildox-Alvarado, E., Charó-Alonso, M. A., de la Peña-Gil, A., & Toro-Vazquez, J. F. (2011). The Effect of Shearing in the Thermo-mechanical Properties of Candelilla Wax and Candelilla Wax-Tripalmitin Organogels. *Food Biophysics*, 6(3), 359–376. <https://doi.org/10.1007/s11483-011-9212-5>
5. Da Silva, E., Bresson, S., & Rousseau, D. (2009). Characterization of the three major polymorphic forms and liquid state of tristearin by Raman spectroscopy. *Chemistry and physics of lipids*, 157(2), 113–119. <https://doi.org/10.1016/j.chemphyslip.2008.11.002>
6. Da Silva, R. C., De Martini Soares, F. A. S., Maruyama, J. M., Dagostinho, N. R., Silva, Y. A., Ract, J. N. R., & Gioielli, L. A. (2016). Microscopic approach of the crystallization of tripalmitin and tristearin by microscopy. *Chemistry and Physics of Lipids*, 198, 1–9. <https://doi.org/10.1016/j.chemphyslip.2016.04.004>
7. Dassanayake, L. S. K., Kodali, D. R., Ueno, S., & Sato, K. (2009). Physical properties of rice bran wax in bulk and organogels. *JAOCS, Journal of the American Oil Chemists' Society*, 86(12), 1163–1173. <https://doi.org/10.1007/s11746-009-1464-6>
8. Dirand, M., Bouroukba, M., Briard, A. J., Chevallier, V., Petitjean, D., & Corriou, J. P. (2002). Temperatures and enthalpies of (solid + solid) and (solid + liquid) transitions of n-alkanes. *Journal of Chemical Thermodynamics*, 34(8), 1255–1277. <https://doi.org/10.1006/jcht.2002.0978>
9. Frank, F., Roberts, T., Snell, J., Yates, C., & Collins, J. (1971). Trimyristin from nutmeg. *Journal of Chemical Education*, 48(4), 255.

- <https://doi.org/10.1021/ed048p255>
10. Haghshenas, N., Smith, P., & Bergenståhl, B. (2001). The exchange rate between dissolved tripalmitin and tripalmitin crystals. *Colloids and Surfaces B: Biointerfaces*, 21(1–3), 239–243. [https://doi.org/10.1016/S0927-7765\(01\)00176-X](https://doi.org/10.1016/S0927-7765(01)00176-X)
 11. Hartel, R. W., von Elbe, J. H., & Hofberger, R. (2018). Fats, Oils and Emulsifiers. In *Confectionery Science and Technology* (pp. 85–124). Springer International Publishing AG. Retrieved from <https://doi.org/10.1007/978-3-319-61742-8>
 12. Hong, B., Li, D., Lei, Q., Xu, L., Fang, W., & Mayama, H. (2012). Kinetics on formation of super water repellent surfaces from phase transformation in binary mixtures of trimyristin and tripalmitin. *Colloids and Surfaces A: Physicochemical and Engineering Aspects*, 396, 130–136. <https://doi.org/10.1016/j.colsurfa.2011.12.056>
 13. Hwang, H. S., Singh, M., Bakota, E. L., Winkler-Moser, J. K., Kim, S., & Liu, S. X. (2013). Margarine from organogels of plant wax and soybean oil. *JAOCS, Journal of the American Oil Chemists' Society*, 90(11), 1705–1712. <https://doi.org/10.1007/s11746-013-2315-z>
 14. Kellens, M., Meeussen, W., & Reynaers, H. (1992). Study of the polymorphism and the crystallization kinetics of tripalmitin: A microscopic approach. *Journal of the American Oil Chemists Society*, 69(9), 906–911. <https://doi.org/10.1007/BF02636342>
 15. Kellens, M., & Reynaers, H. (1992). Study of the polymorphism of saturated monoacid triglycerides I: melting and crystallization behaviour of tristearin. *Lipid/Fett*, 94(3), 94–100. <https://doi.org/10.1002/lipi.19920940304>
 16. Kerr, R. M., Tombokan, X., Ghosh, S., & Martini, S. (2011). Crystallization behavior of anhydrous milk fat–sunflower oil wax blends. *Journal of agricultural and food chemistry*, 59(6), 2689–2695. <https://doi.org/10.1021/jf1046046>
 17. Kolbe, E., Wilson, L. A., & Hartel, R. (1999). A round robin evaluation of differential scanning calorimetry to measure transition enthalpy and temperatures. *Journal of food engineering*, 40(1-2), 95–99. [https://doi.org/10.1016/S0260-8774\(99\)00044-8](https://doi.org/10.1016/S0260-8774(99)00044-8)
 18. Magill, J. H. (2001). Review spherulites: A personal perspective. *Journal of Materials Science*, 36(13), 3143–3164. <https://doi.org/10.1023/A:1017974016928>
 19. Marangoni, A. G., Acevedo, N., Maleky, F., Co, E., Peyronel, F., Mazzanti, G., Pink, D. (2012). Structure and functionality of edible fats. *Soft Matter*, 8(5), 1275–1300. <https://doi.org/10.1039/c1sm06234d>

20. Martini, S., Carelli, A. A., & Lee, J. (2008). Effect of the addition of waxes on the crystallization behavior of anhydrous milk fat. *Journal of the American Oil Chemists' Society*, *85*(12), 1097-1104. <https://doi.org/10.1007/s11746-008-1310-2>
21. Matovic, M., van Miltenburg, J. C., Los, J., Gandolfo, F. G., & Flöter, E. (2005). Thermal properties of tristearin by adiabatic and differential scanning calorimetry. *Journal of Chemical & Engineering Data*, *50*(5), 1624-1630. <https://doi.org/10.1021/je050092d>
22. Ostuni, E., Kamaras, P., & Weiss, R. G. (1996). Novel x-ray method for in situ determination of gelator strand structure: Polymorphism of cholesteryl anthraquinone-2-carboxylate. *Angewandte Chemie (International Edition in English)*, *35*(12), 1324–1326. <https://doi.org/10.1002/anie.199613241>
23. Patel, A. R. (2015). Alternative Routes to Oil Structuring, 15–27. <https://doi.org/10.1007/978-3-319-19138-6>
24. Ramírez-Gómez, N. O., Acevedo, N. C., Toro-Vázquez, J. F., Ornelas-Paz, J. J., Dibildox-Alvarado, E., & Pérez-Martínez, J. D. (2016). Phase behavior, structure and rheology of candelilla wax/fully hydrogenated soybean oil mixtures with and without vegetable oil. *Food Research International*, *89*, 828-837. <https://doi.org/10.1016/j.foodres.2016.10.025>
25. Sánchez-Becerril, M., Marangoni, A. G., Perea-Flores, M. J., Cayetano-Castro, N., Martínez-Gutiérrez, H., Andraca-Adame, J. A., & Pérez-Martínez, J. D. (2018). Characterization of the micro and nanostructure of the candelilla wax organogels crystal networks. *Food structure*, *16*, 1-7. <https://doi.org/10.1016/j.foostr.2018.02.001>
26. Sato, K. (2001). Sato Crystallization behaviour of fats and lipids. *Chemical Engineering Science*, *56*, 2255–2265. [https://doi.org/10.1016/S0009-2509\(00\)00458-9](https://doi.org/10.1016/S0009-2509(00)00458-9)
27. Serrato-Palacios, L. L., Toro-Vazquez, J. F., Dibildox-Alvarado, E., Aragón-Piña, A., Morales-Armenta, M. D. R., Ibarra-Junquera, V., & Pérez-Martínez, J. D. (2015). Phase behavior and structure of systems based on mixtures of n-hentriacontane and melissic acid. *JAOCs, Journal of the American Oil Chemists' Society*, *92*(4), 533–540. <https://doi.org/10.1007/s11746-015-2623-6>
28. Shearer, H. M. M. , & Vand, V. (1956). The crystal structure of the monoclinic form of n-hexadecanol. *Acta Crystallographica*, *13*(10), 770–774. <https://doi.org/10.1107/S0365110X60001862>
29. Small, D. M. (1986). The physical chemistry of lipids: from alkanes to phospholipids. In D. J. Hanahan (Ed.), *Handbook of Lipid Research* (Plenum Pre, pp. 367–372). New York.

30. Son, J. M., Lee, K. T., Akoh, C. C., Kim, M. R., Kim, M. J., & Lee, J. H. (2010). Optimisation of tripalmitin-rich fractionation from palm stearin by response surface methodology. *Journal of the Science of Food and Agriculture*, 90(9), 1520–1526. <https://doi.org/10.1002/jsfa.3978>
31. Timms, R. E. (1984). Phase behaviour of fats and their mixtures. *Progress in Lipid Research*, 23(1), 1–38. [https://doi.org/10.1016/0163-7827\(84\)90004-3](https://doi.org/10.1016/0163-7827(84)90004-3)
32. Toro-Vazquez, J. F., Mauricio-Pérez, R., González-Chávez, M. M., Sánchez-Becerril, M., Ornelas-Paz, J. de J., & Pérez-Martínez, J. D. (2013). Physical properties of organogels and water in oil emulsions structured by mixtures of candelilla wax and monoglycerides. *Food Research International*, 54(2), 1360–1368. <https://doi.org/10.1016/j.foodres.2013.09.046>
33. Toro-Vazquez, J. F., Morales-Rueda, J. A., Dibildox-Alvarado, E., Charó-Alonso, M., Alonzo-Macias, M., & González-Chávez, M. M. (2007). Thermal and textural properties of organogels developed by candelilla wax in safflower oil. *JAOCS, Journal of the American Oil Chemists' Society*, 84(11), 989–1000. <https://doi.org/10.1007/s11746-007-1139-0>
34. Toro Vazquez, J. F., & Pérez Martínez, J. D. (2018). Thermodynamic Aspects of Molecular Gels. In W. Richard G (Ed.), *Molecular Gels: Structure and Dynamics* (pp. 57–87). Retrieved from <https://dx.doi.org/10.1039/9781788013147-00057>
35. Walstra, P. (2003). *Physical Chemistry of Foods*. New York: CRC Press.
36. Yang, S., Li, G., Saleh, A. S. M., Yang, H., Wang, N., Wang, P., Xiao, Z. (2017). Functional Characteristics of Oleogel Prepared from Sunflower Oil with β -Sitosterol and Stearic Acid. *JAOCS, Journal of the American Oil Chemists' Society*, 94(9), 1153–1164. <https://doi.org/10.1007/s11746-017-3026-7>
37. Zetzi, A. K., & Marangoni, A. G. (2014). Structured Emulsions and Edible Oleogels as Solutions to Trans Fat. In D. R. Kodali (Ed.), *Trans Fats Replacement Solutions* (pp. 215–243). Urbana, Illinois. <https://doi.org/10.1108/eb059455>

FIGURE 1

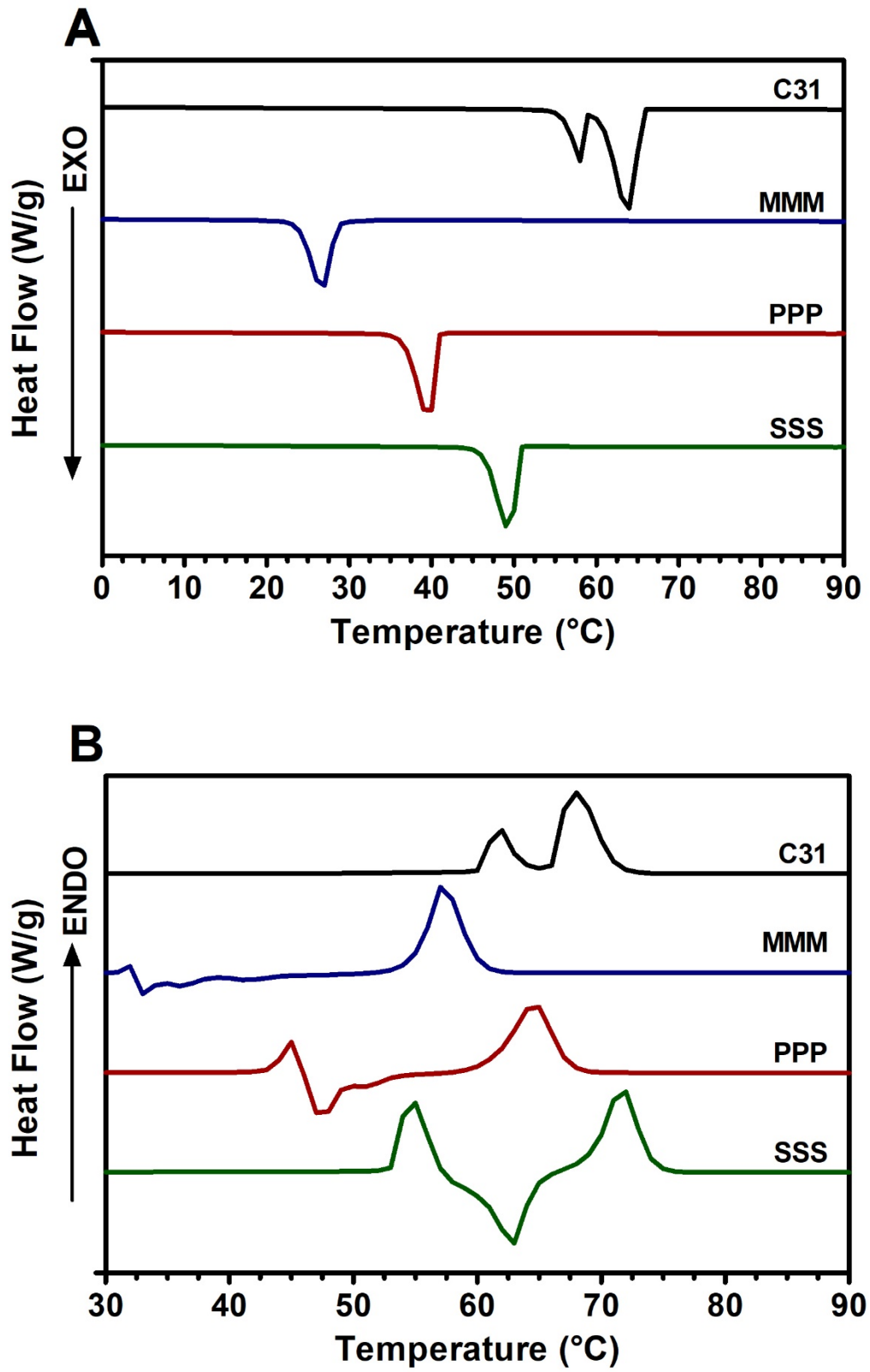


FIGURE 2

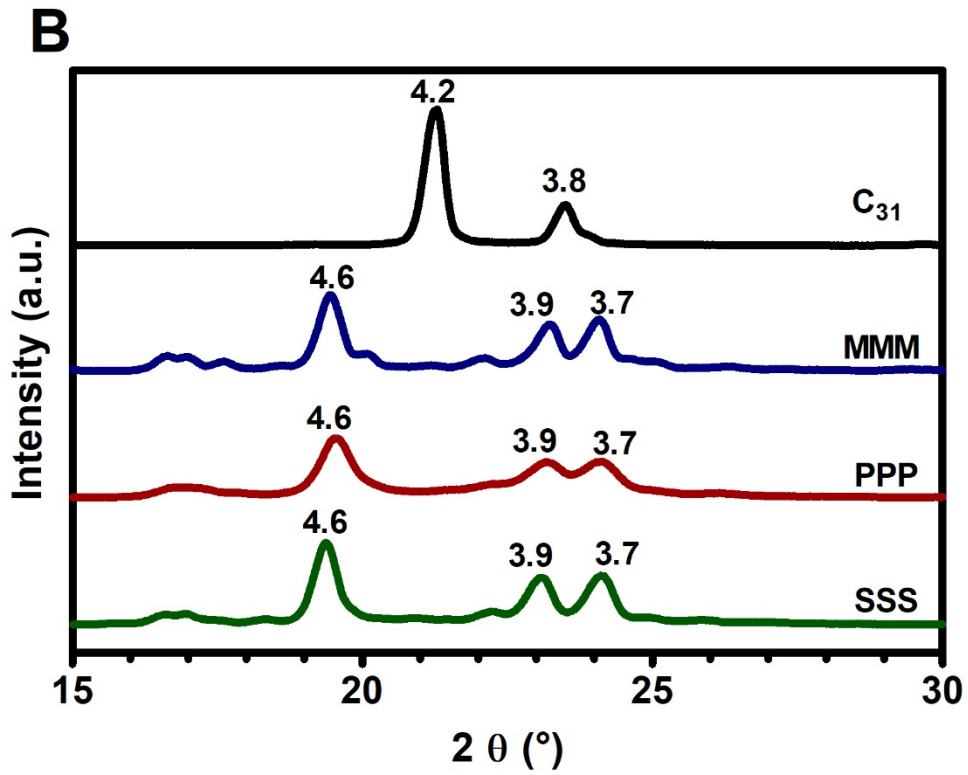
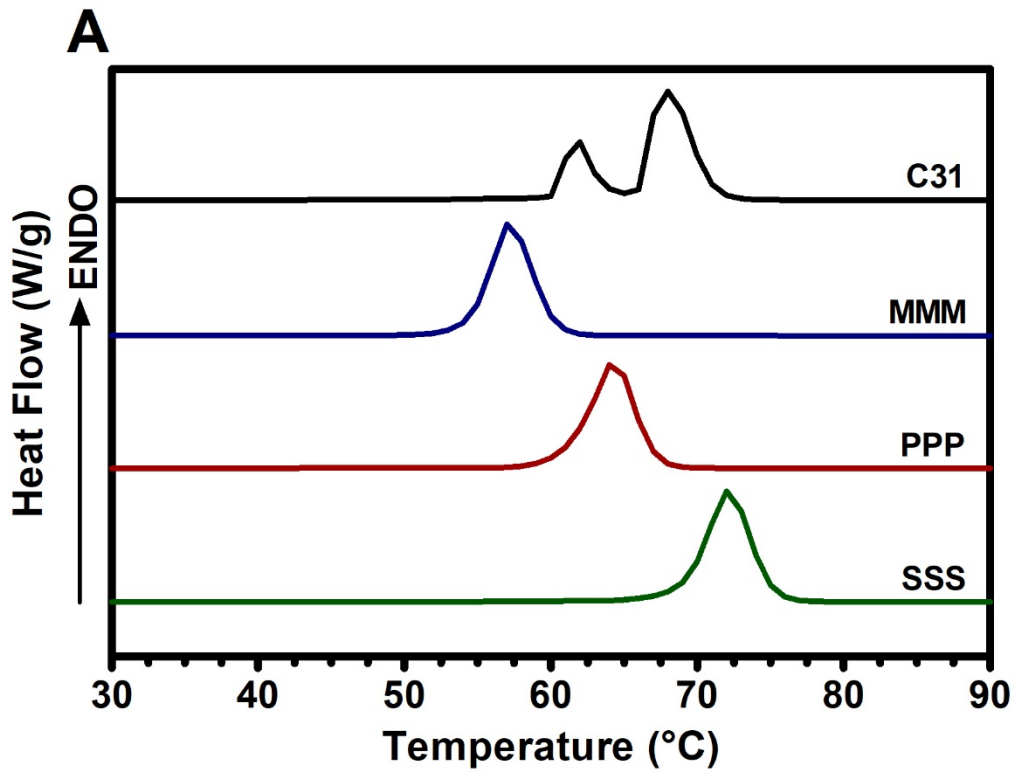


FIGURE 3

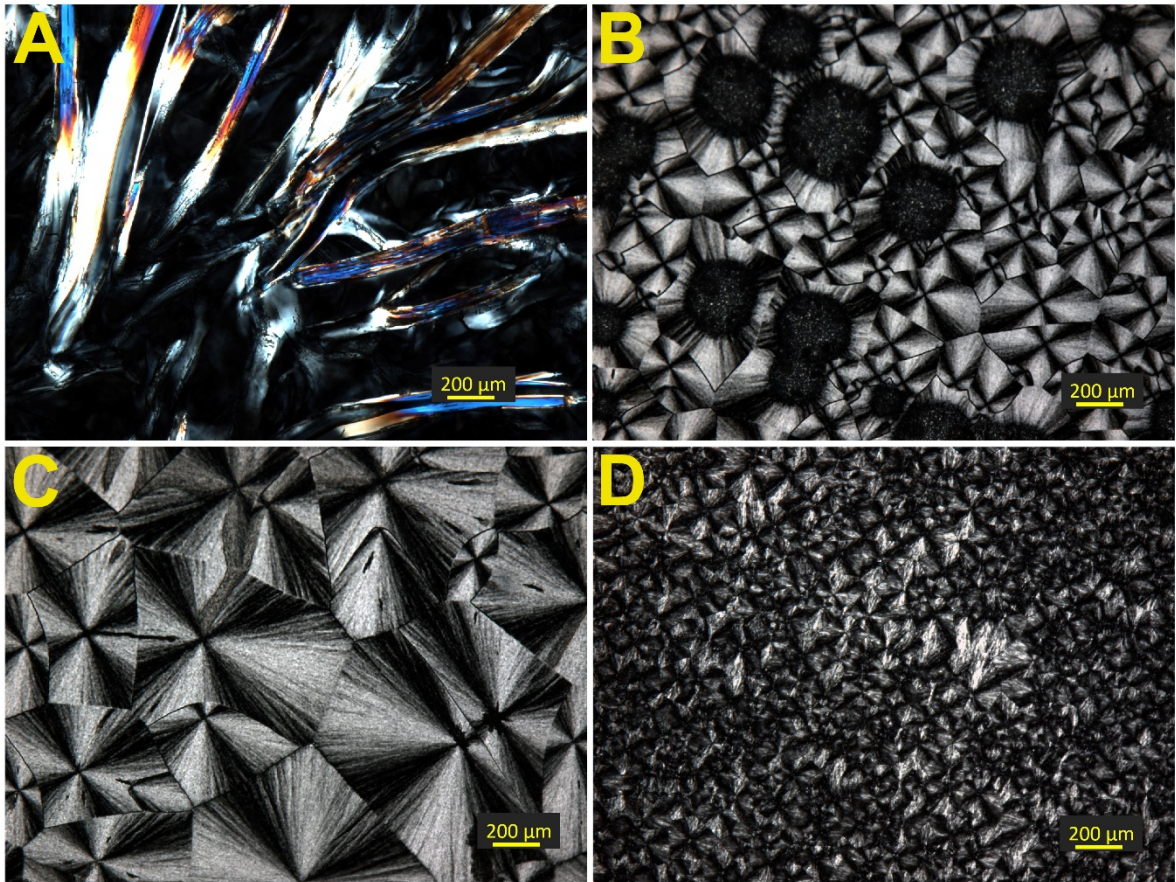


FIGURE 4

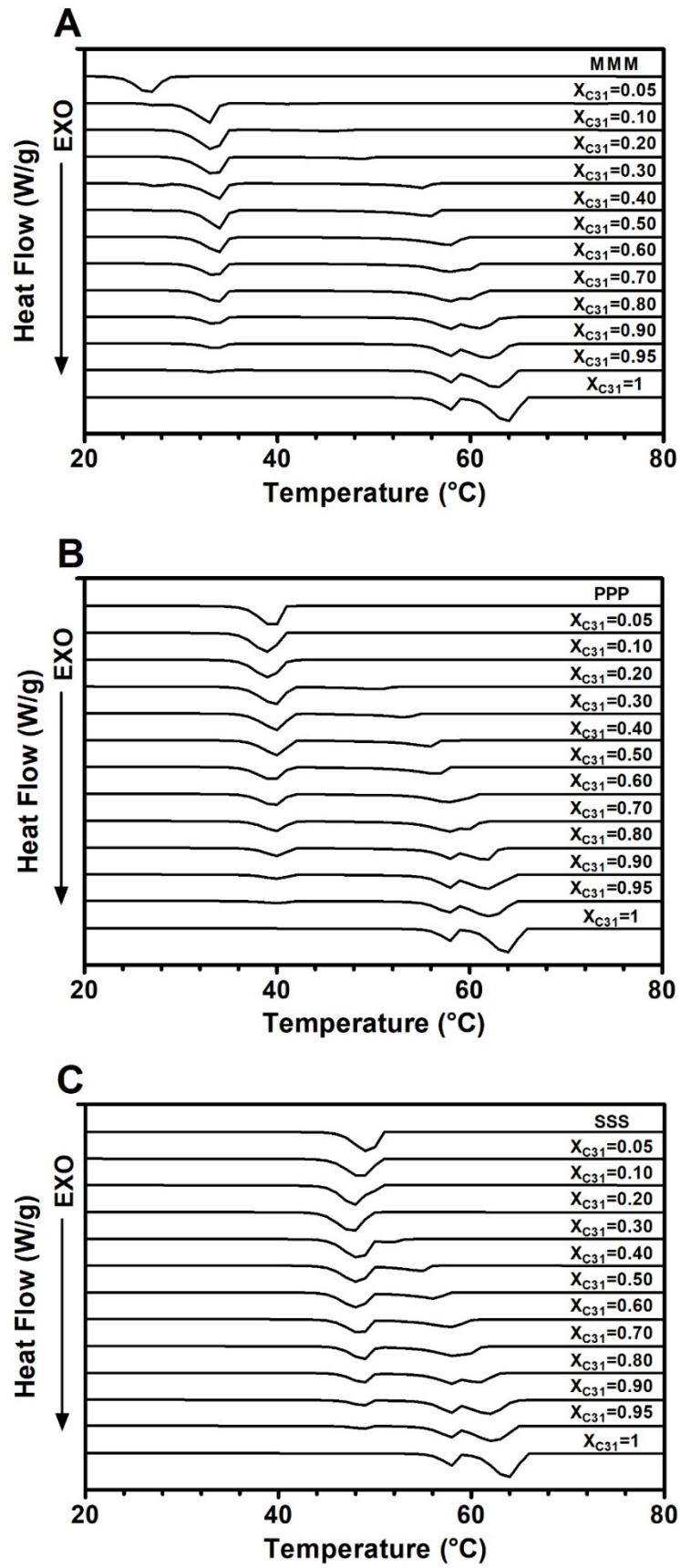


FIGURE 5

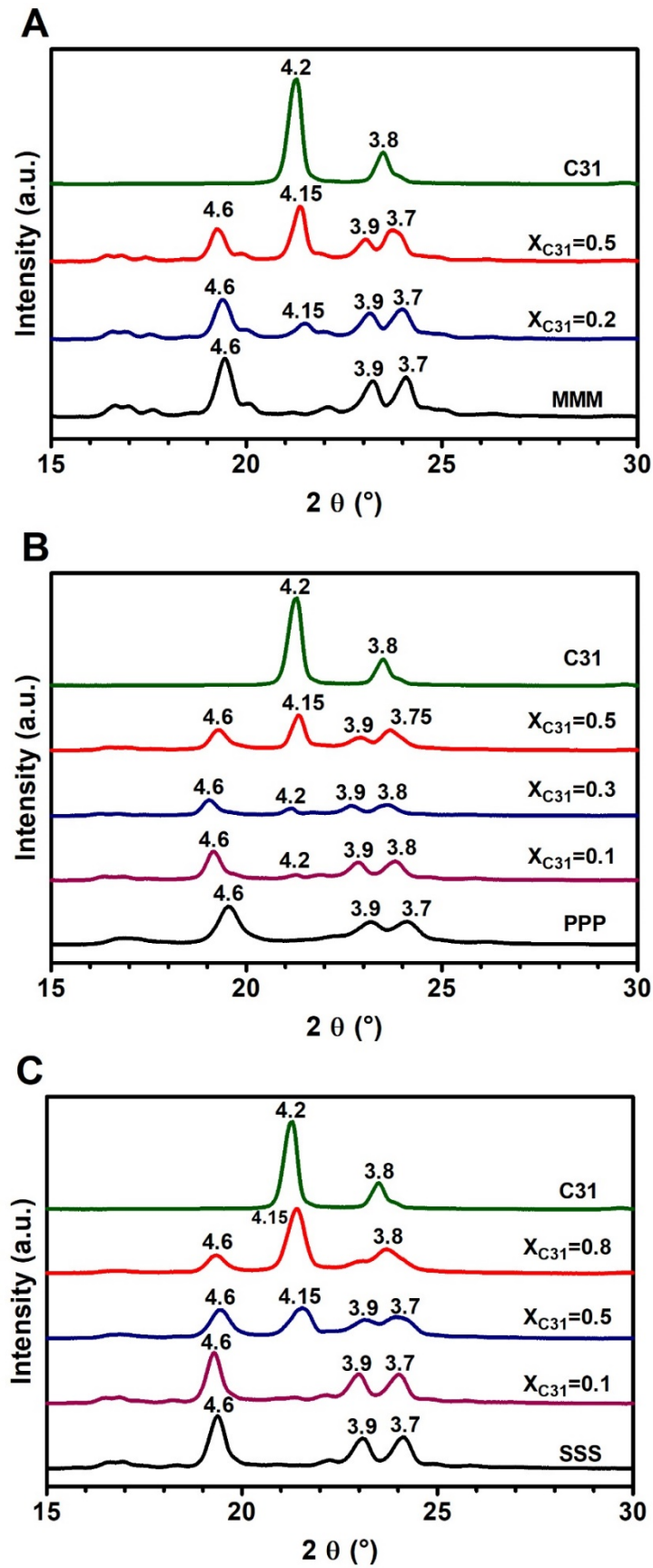


FIGURE 6

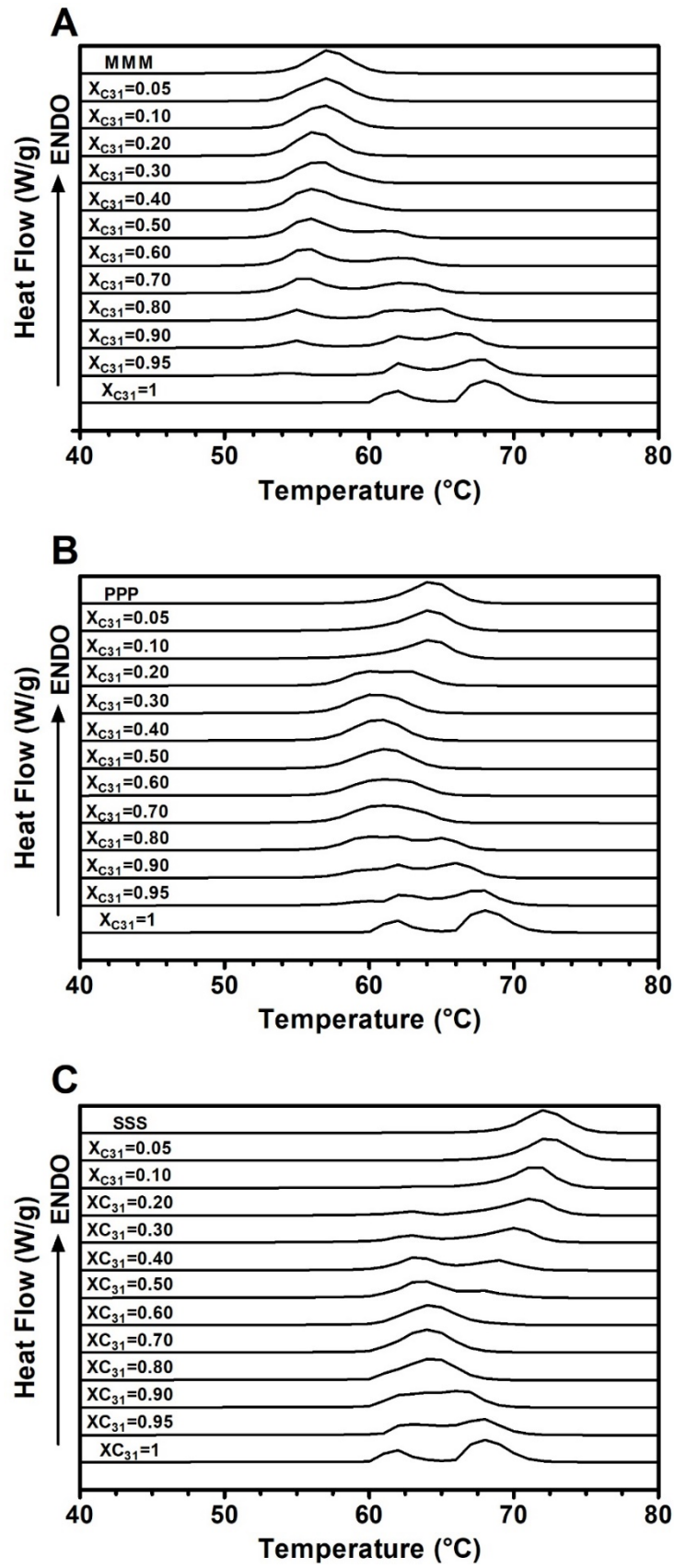
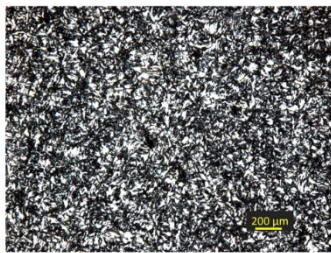
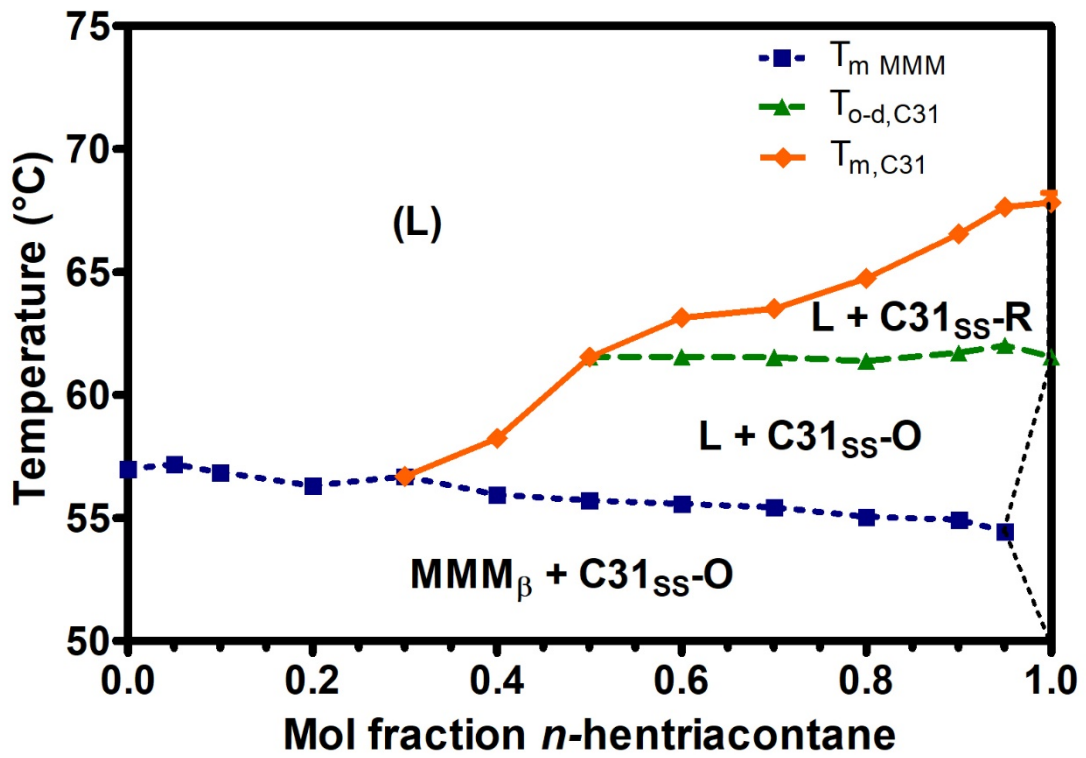
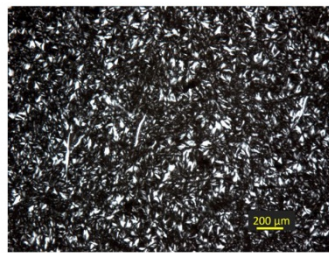


FIGURE 7



$X_{C31}=0.20$

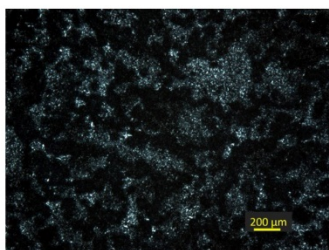
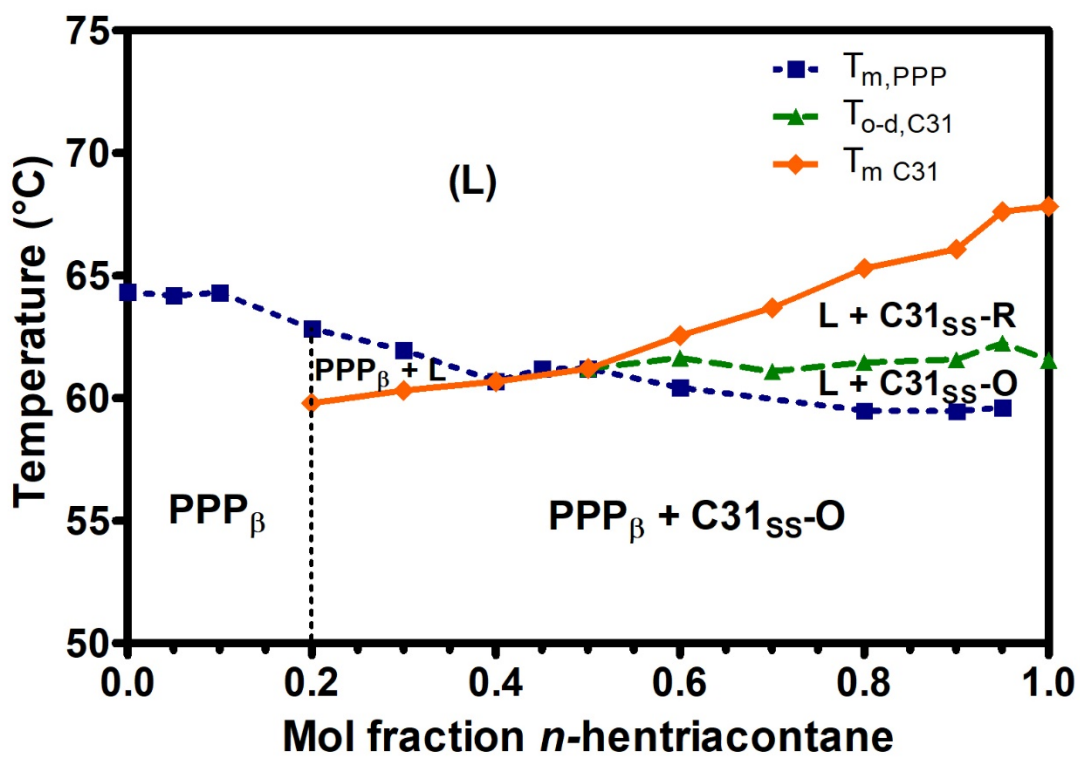


$X_{C31}=0.30$



$X_{C31}=0.60$

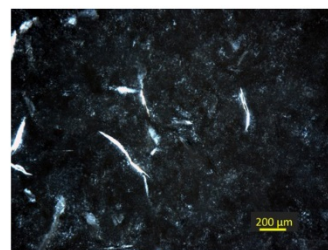
FIGURE 8



$X_{C31} = 0.20$

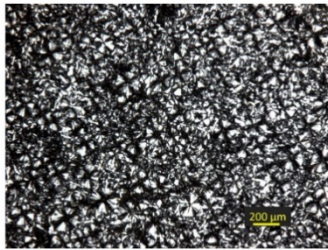
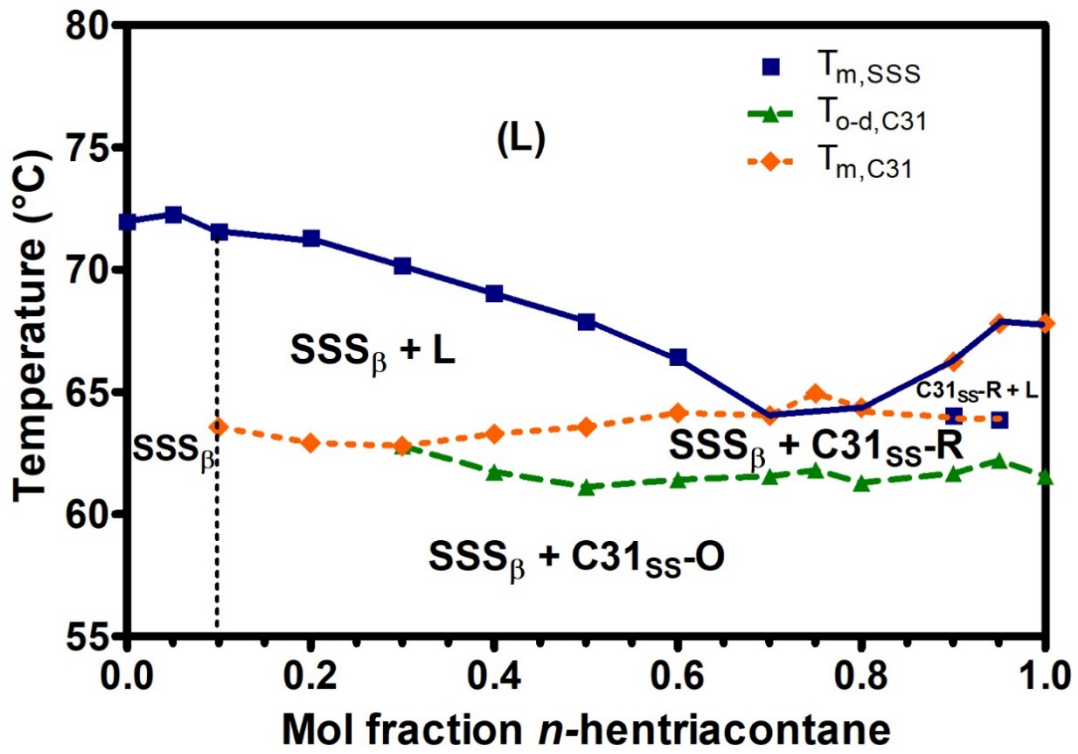


$X_{C31} = 0.50$

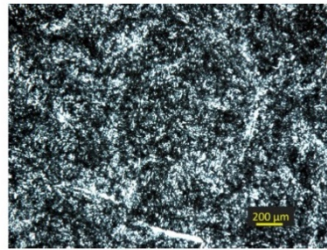


$X_{C31} = 0.60$

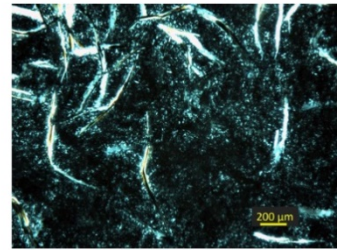
FIGURE 9



$X_{C31} = 0.10$



$X_{C31} = 0.40$



$X_{C31} = 0.80$

FIGURE S1

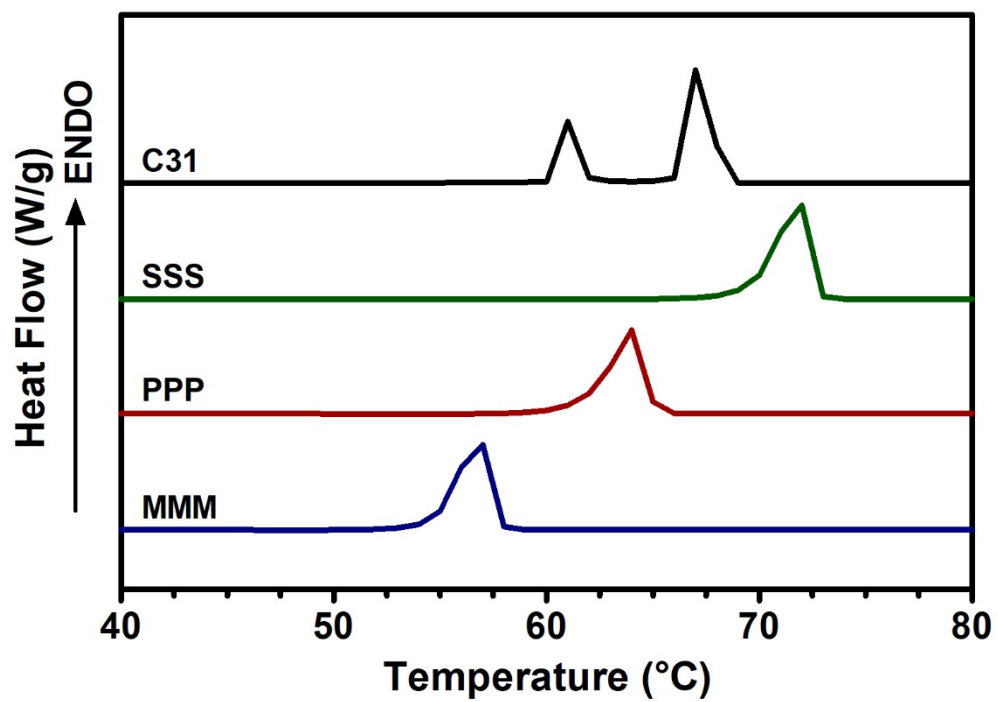


FIGURE S2

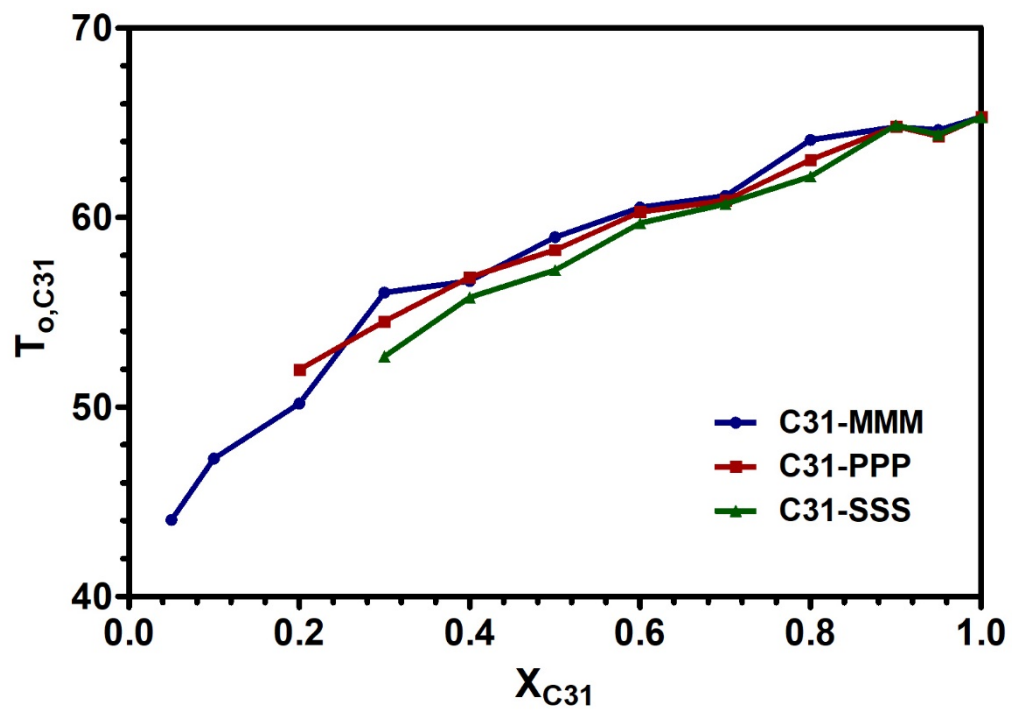


FIGURE S3

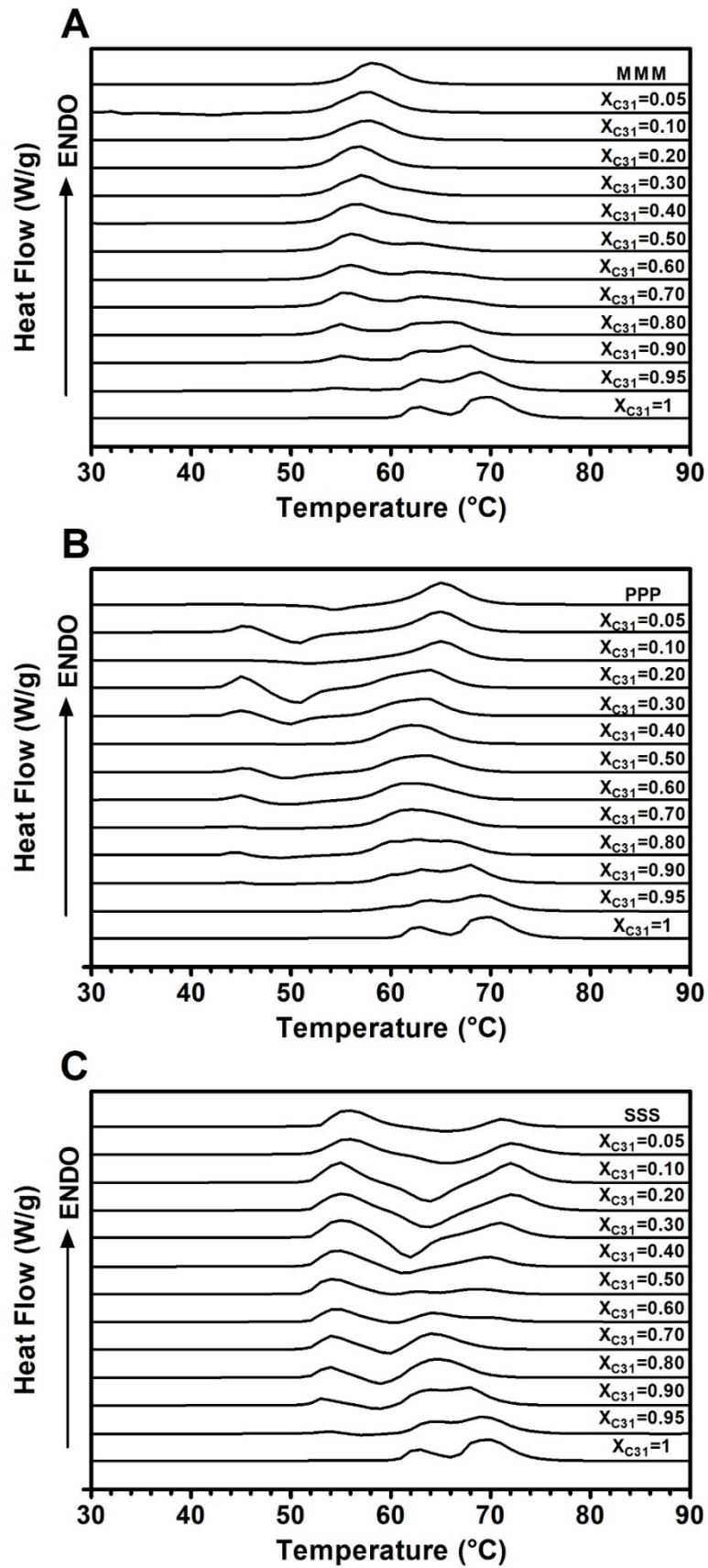


FIGURE S4

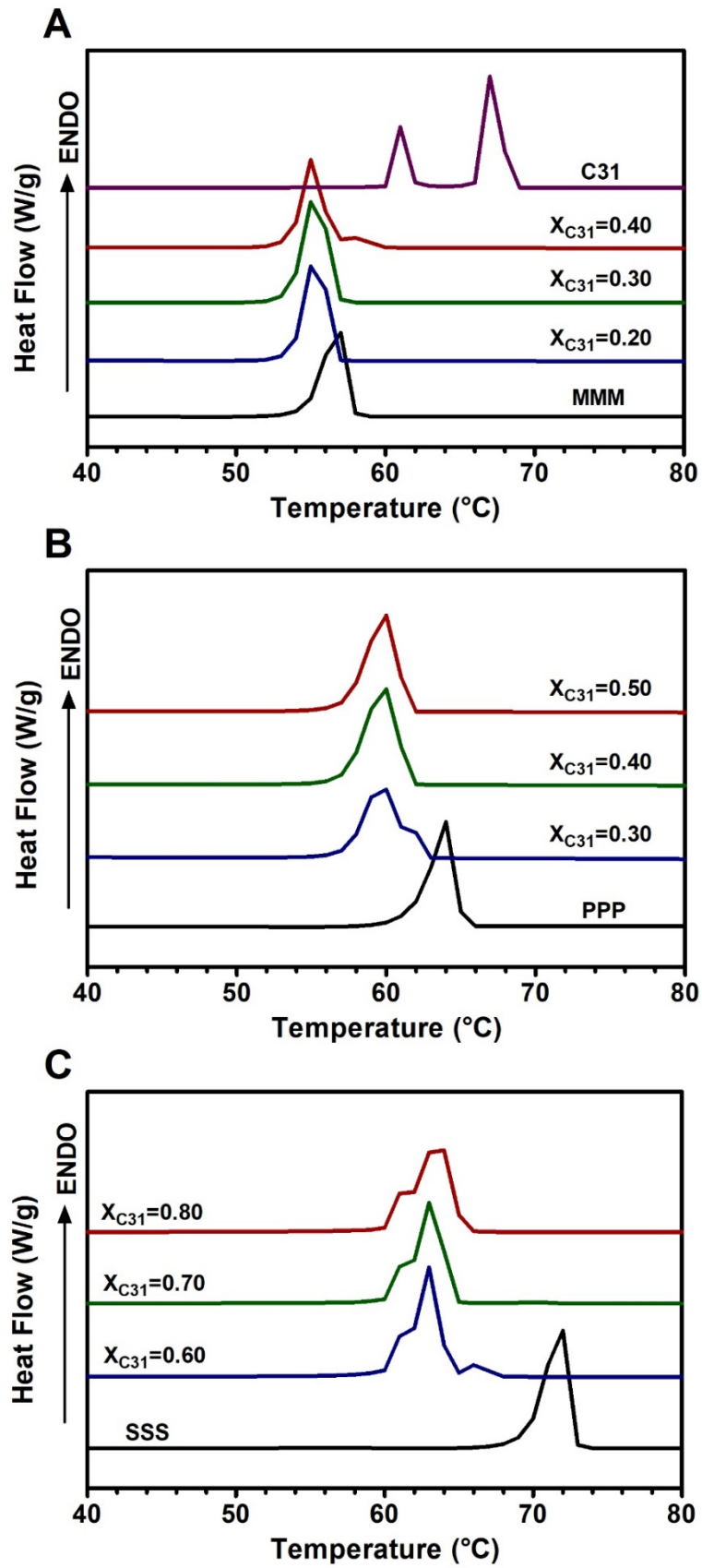


Table 1. Melting temperatures and enthalpies for pure triacylglycerides after the annealing process for the polymorphic β form.

TAGs	T_m^a (°C)	ΔH_m^a (J/g)	T_m^b (°C)	ΔH_m^b (J/g)	T_m (°C)	ΔH_m (J/g)
MMM	56.99 ± 0.02	182.45 ± 10.11	56.00 – 58.50	188.13		
	64.33 ± 0.08	188.65 ± 1.63	66.00 – 66.4	203.82	65.8 ^f	190.69 ^f
PPP	71.97 ± 0.37	190.95 ± 3.46	73.00 – 73.50	213.24	72.4 ± 0.05 ^e ,	217 ± 1.6 ^e , 219.6 ^d ,
SSS					71.2 ^f	211.1 ^e , 213.13 ^f

(a) Experimental data; (b) Hartel *et al.*, 2018; (c) Da Silva *et al.*, 2009; (d) Matovic., 2005; (e) Kolbe *et al.*, 1999; (f) Kellens and Reynaers., 1992.

Table 2. Experimental temperatures of the solid-liquid equilibrium in the binary mixture C31 (1) + MMM (2).

X_{C31}	<i>Liquidus line</i>	<i>Solidus line</i>	<i>The o-d solid transition line</i>
	$T_{m,C31}$	$T_{m,MMM}$	$T_{od,C31}$
0		56.99 ± 0.02	
0.05		57.18 ± 0.33	
0.10		56.86 ± 0.46	
0.20		56.30 ± 0.08	
0.30	58.22 ± 0.05	56.69 ± 0.08	
0.40	58.23 ± 0.18	55.94 ± 0.57	
0.50	61.53 ± 0.16	55.71 ± 0.01	
0.60	63.15 ± 0.13	55.57 ± 0.16	61.55 ± 0.26
0.70	63.50 ± 0.07	55.44 ± 0.13	61.53 ± 0.05
0.80	64.75 ± 0.02	55.04 ± 0.05	61.38 ± 0.08
0.90	66.55 ± 0.02	54.94 ± 0.05	61.70 ± 0.00
0.95	67.65 ± 0.09	54.45 ± 0.18	62.01 ± 0.08
1	67.82 ± 0.56		61.55 ± 0.35

Table 3. Experimental temperatures of the solid-liquid equilibrium in the binary mixture C31 (1) + PPP (2).

X_{C31}	<i>Liquidus line</i>		<i>Solidus line</i>		<i>The o-d solid transition line</i> $T_{od,C31}$
	T_{m_i}	<i>i</i>	T_{m_i}	<i>i</i>	
0	64.33 ± 0.08	PPP			
0.05	64.19 ± 0.11	PPP			
0.10	64.30 ± 0.19	PPP			
0.20	62.84 ± 0.21	PPP	59.80 ± 0.09	C31	
0.30	61.96 ± 0.00	PPP	60.32 ± 0.08	C31	
0.40	60.69 ± 0.01	C31 & PPP	60.69 ± 0.01	C31 & PPP	
0.45			61.19 ± 0.33	PPP	
0.50	61.20 ± 0.06	C31 & PPP	61.20 ± 0.06	C31 & PPP	
0.60	62.56 ± 0.94	C31	60.42 ± 0.62	PPP	61.63 ± 0.07
0.70	63.70 ± 0.02	C31			61.08 ± 0.91
0.80	65.29 ± 0.03	C31	56.49 ± 0.03	PPP	61.45 ± 0.04
0.90	66.08 ± 0.29	C31	59.46 ± 0.06	PPP	61.57 ± 0.21
0.95	67.61 ± 0.10	C31	59.61 ± 0.06	PPP	62.24 ± 0.13
1	67.82 ± 0.56	C31			61.55 ± 0.35

Table 4. Experimental temperatures of the solid-liquid equilibrium in the binary mixture C31 (1) + SSS (2).

X_{C31}	Liquidus line		Solidus line		The o-d solid transition line
	T_{m_i}	i	T_{m_i}	i	$T_{od,C31}$
0	71.97 ± 0.37	SSS			
0.05	72.27 ± 0.25	SSS			
0.10	71.56 ± 0.02	SSS	63.56 ± 0.51	C31	
0.20	71.29 ± 0.21	SSS	62.92 ± 0.34	C31	
0.30	70.18 ± 0.37	SSS	62.79 ± 0.29	C31	
0.40	69.04 ± 0.16	SSS	63.29 ± 0.08	C31	61.73 ± 0.26
0.50	67.88 ± 0.08	SSS	63.56 ± 0.08	C31	61.11 ± 0.06
0.60	66.43 ± 0.08	SSS	64.14 ± 0.01	C31 & SSS	61.42 ± 0.02
0.70	64.04 ± 0.46	C31 & SSS	64.04 ± 0.46	C31 & SSS	61.55 ± 0.64
0.75			64.94 ± 0.18	C31	61.80 ± 0.11
0.80	64.35 ± 0.10	C31 & SSS	64.35 ± 0.10	C31 & SSS	61.28 ± 0.01
0.90	66.24 ± 0.04	C31	64.03 ± 0.19	SSS	61.67 ± 0.22
0.95	67.79 ± 0.00	C31	63.87 ± 0.48	SSS	62.19 ± 0.03
1	67.82 ± 0.56	C31			61.55 ± 0.35